CHAPTER 4

Direct observation of laser induced phase objects

Laser pulse focusing in the bulk of transparent materials induces a localized change of the refractive index. In this chapter, we discuss the influence of several irradiation conditions on the optical properties of the laser affected region. The investigations are carried out in a-SiO_2 and BK7. Those two materials were selected because of their very different properties (e.g. different transition points, different thermal expansion coefficients). After irradiation, the samples are observed under a phase contrast microscope allowing for a visualization of the real part of the refractive index map imprinted by the laser pulses. Complementary investigations in optical transmission microscopy are also presented. They give additional information regarding the transparency of the laser induced traces. Hence, altogether, phase contrast microscopy (PCM) and optical transmission microscopy (OTM) provide a characterization of the complex refractive index changes experienced by the material. Different irradiation conditions are explored.

In Sec. 4.1.3, we observe the refractive index changes induced by focusing a single laser pulse in the bulk of a-SiO_2 and BK7 under standard ultrafast irradiation conditions. We attempt to correlate the morphology of the laser-induced trace observed in PCM with the spatial distribution of energy deposition predicted by the nonlinear propagation equation presented in Sec. 2.4.1. The influence of the laser pulse energy is also studied, as well as the consequences of spherical aberrations. Section 4.2 contains experimental observations corresponding to multipulse irradiation conditions. The effect of the number of pulses per site and also of the arrival time between two consecutive pulses is investigated. Finally, in Sec. 4.3 the laser pulse duration is taken as a free parameter. Studies are carried out with

laser pulse durations between $\sim$ 100 fs up to a few picoseconds. In order to tune the pulse duration, the laser pulses are linearly chirped. The influence of the laser pulse duration and the chirp direction on the modification threshold and on the properties of the final laser-induced objects is studied.

4.1 Single pulse irradiation at various laser-pulse energies

4.1.1 Energy dependence study in amorphous fused silica

Experimental conditions

The laser used in this section is system II (τ=90 fs). The laser beam is focused with the objective described in Sec. 3.4.2 (NA=0.45). The paraxial focusing plane is carefully fixed at a distance D such as $170 < D < 210\mu$m in order to minimize the influence of spherical aberrations, as explained in Sec. 3.2.2. We recall (see Sec. 3.4.4) that a positive phase contrast microscope is used, implying that a phase object with a refractive index higher than the bulk refractive index appears darker than the background.

PCM and OTM observations in a-SiO_2

Phase contrast microscopy (PCM) and optical transmission microscopy (OTM) observations of laser-induced tracks in amorphous fused silica (a-SiO_2) are presented in Fig. 4.1. Noticeably, every track exhibits a dark region (of higher refractive index than the bulk) and also one or several white features, depending on the laser pulse energy. Nevertheless, from the analysis of Fig. 4.1, two regimes of interaction emerge: a soft mode, for input energies lower than 2.5 μJ and a strong interaction mode, for energies higher than 6 μJ. The strong regime of interaction is characterized by the onset of a black stain around a white region.

Discussion: interaction in the bulk of a-SiO_2 at low laser pulse energies

In this section, we discuss the aspect of the laser generated imprints visible in Fig. 4.1 for laser energies lower than 2 μJ. Low laser pulse energies and tight focusing are typically used in the frame of technological applications [68, 75, 76, 77].

In this regime, the length of the trace scales with the input energy but the general morphology is conserved. Therefore, we base our discussion on the 1 μJ trace presented in Fig. 4.2.

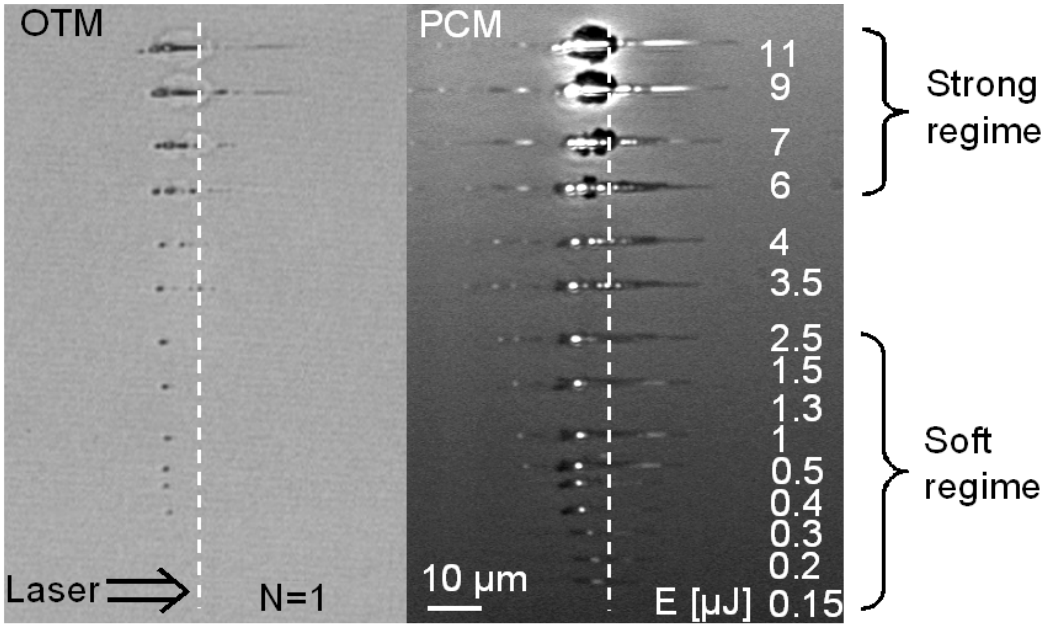

Figure 4.1: Phase contrast microscopy (PCM) and optical transmission microscopy (OTM) observations of laser-induced traces by a single pulse in amorphous fused silica for various laser beam energies. On the right column, laser pulse energies in μJ are specified. The dot line represents the estimated focal plane.

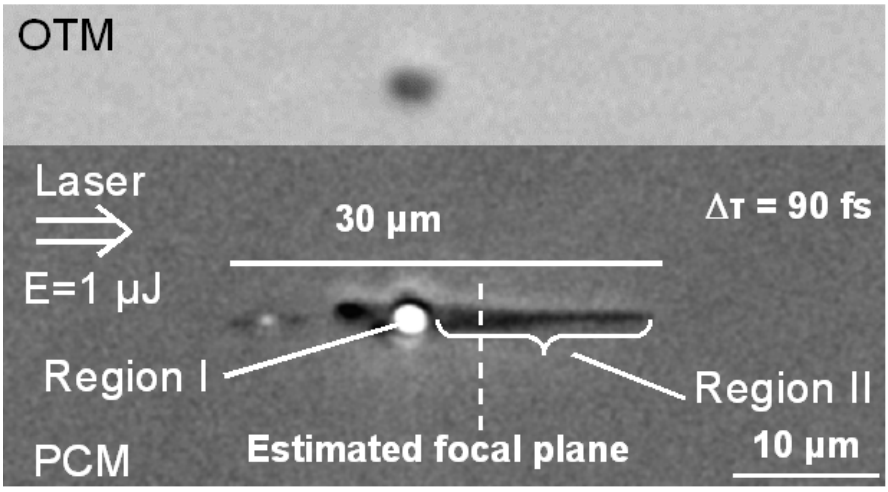

Figure 4.2: Phase-contrast microscopy (PCM) and optical transmission microscopy (OTM) observation of a single-pulse laser modification trace in fused silica for an input energy of 1 μJ. The dot line represents the estimated focal plane. A black region is observed around the focal area and a white dot is formed on the tail of the structure.

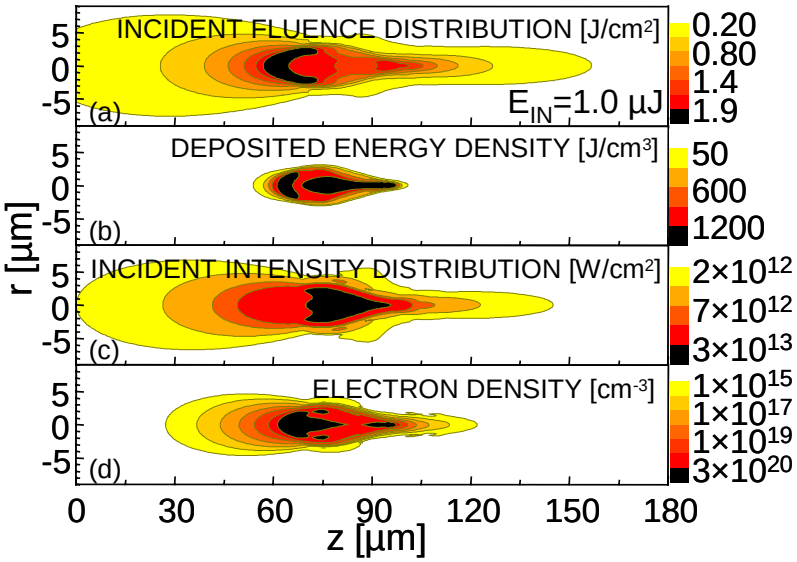

Figure 4.3: Simulation of energy deposition into in fused silica at the end of the 120 fs irradiation pulse. (a) incident fluence (J/cm^2); (b) absorbed energy (J/cm^3); (c) peak intensity distribution (W/cm^3); (d) electronic density (cm^{-3}) 50 fs after the pulse center.

We propose to correlate the spatial distribution of energy deposition obtained when solving the nonlinear Schrödinger equation (NLSE) presented in Eq. 2.32 with the PCM pictures. The discussion is restricted here to the description of the most striking features observed and to their probable origin. From the abundance of relevant informations gathered when solving Eq. 2.32 (see [34]), we select and present on Fig. 4.3 solely the overall incident fluence distribution, the total deposited energy density, the incident intensity distribution and the final electronic density at the end of the irradiation sequence (50fs after the center of the pulse) for the present discussion.

As a general comment, the interaction mostly takes place outside of the focal plane. Despite of the tight focusing conditions, the material is modified over a region of about 30 μm. A simulation of the time-resolved energy deposition in the free carriers during the pulse propagation (not shown here) reveals that this energy spread is mostly due to defocusing of the trailing edge of the pulse on the electron-hole plasma formed by the leading edge of the laser pulse.

Firstly, we discuss the mechanism of void formation (region I). The maximal fluence region in Fig. 4.3 (a) can unmistakably be associated to the white sphere observed in PCM (domain I in Fig. 4.2). From OTM analysis, domain I is not fully transparent. This prevents us from being absolutely affirmative regarding the final refractive index of this region. Nevertheless, based on observations by several groups [78, 79, 80] we can reasonably state that this

sphere is actually an empty void and that the dark aspect in OTM is justified by the strong refractive index gradient between the cavity and the surrounding bulk. Considering that the deposited energy density is about 1200 J/cm^{-3} (see Fig. 4.3 (b)) within a 2 μm sphere, the corresponding temperature rise is about 700 °C, well below the melting point of fused silica (about 1830 °C). Although the value of 700 °C has to be taken with a certain precaution, considering the uncertainties in the NLSE approach, this relatively low temperature suggests that the mechanism of void formation is not a result from conventional vaporization. Instead, as region I corresponds to a zone of high energy deposition, the presence of void may rather be associated to a strong thermal expansion. Upon cooling, the material does not return in its original configuration and a region of low density persists.

The formation of region II has plausibly a very different origin. According to Fig. 4.3 (c), region II results from the propagation of a very intense pulse. Interestingly, a comparison between Fig. 4.3 (a) and (c) shows that this high intensity seems to be due to a pulse compression mechanism rather than to an energy increase. In some areas of region II, the amount of energy deposited is high whereas the electron density is not maximal. This indicates a high energy load per electron favoring further ionization by collisional process and possibly self trapped exciton (STE) formation. The decay of STE results in point defect formation with consequences on the refractive index (cf Sec. 2.5.2). Depending on the density of nano-dislocations, a structural relaxation may take place and lead to a high density region.

As a conclusion, we assign the appearance of region I to the formation of a void whereas the positive refractive index visible in region II is attributed to lattice softening and subsequent dislocations on a nanometer scale.

Discussion: imprints induced with high input energies

As the regime of soft interaction was discussed in the previous section, the regime of strong interaction, i.e. for laser energies higher than 5.5 μJ (see Fig. 4.2) is discussed in this section. Our analysis is based on typical pictures of this interaction regime, shown in Fig. 4.4.

This regime of interaction is characterized by the onset of a black stain visible in PCM around the focal region, transparent in OTM and labeled as region IV. The rest of the discussion focuses on a possible scenario for the formation of region IV. This high refractive index region is plausibly the result of a shock wave induced densification, resulting in a change of connectivity of the SiO_2 tetrahedra forming the glass matrix (see Sec. 2.5.3). As shown by recent molecular studies [51], shock wave propagation results in an increase of 3-4 and 8-10 membered rings. The observation of material modification triggered by a shock wave is in good agreement with high NA experiments [81, 82]. Although no simulation results are available at those high energies, the following scenario is proposed.

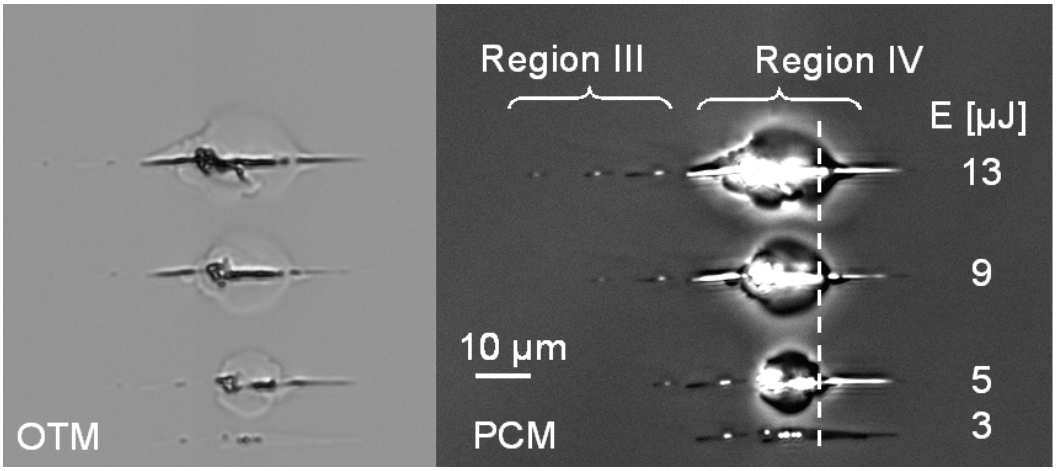

Figure 4.4: Phase-contrast observation of single-pulse laser modification trace in silica in the strong regime of interaction and comparison with optical transmission microscopy analysis (left side). The dotted line represents the estimated focal plane.

The energy deposition is essentially concentrated around the axis, in a confined volume appearing in white in PCM. After energy transfer from the electronic bath to the lattice, the material is left in an extreme thermodynamic state characterized by a significant pressure and temperature. This high pressure exceeds the bulk modulus and the energy dissipates in of a shock wave, with dramatic consequences on the local structure of the material. This mechanical wave is gradually damped, converting its energy into a plastic deformation of the surrounding material. The sharp boundary of the black stain defines the shock-affected volume and corresponds to the location where the pressure exerted by the shock wave is equal to the internal pressure of the cold material [82].

A higher limit for the maximum density of the shock affected volume can be deduced from simple mass conservation considerations, assuming that all silicon and oxygen atoms have been transfered from the white region to the black region in PCM. Under those conditions, the density of the shock affected volume would be of about 2.30 g.cm^{-3}. The subsequent refractive index change can be approximated to about 3% by applying (see [83] and references therein):

$$\frac{\partial n}{n} = 0.4505 \frac{\partial \rho}{\rho} \tag{4.1}$$

where ρ and n correspond to the density and refractive index of the pristine bulk (respectively 1.45 and 2.20 g.cm^{-3} for fused silica).

The region labeled III in Fig. 4.4 shows a very different morphology and denotes a different interaction mode. The filaments emphasized in Fig. 4.4 show an interesting similarity with low energy traces. Therefore, we suggest that those filaments have been imprinted by back

propagating light. This implies that a sufficient amount of energy from the tail of the pulse has been reflected on the electron-hole plasma mirror formed by the leading edge of the pulse. The succession of on-axis dots observable in the highest laser pulse energy conditions may indicate that the back propagating pulse undergoes sequentially several collapses and plasma defocusing. Another possibility could also be a stationary interference with the end of the incoming pulse. It is a challenging point to address theoretically because of the multitude of phenomena involved simultaneously. One can speculate that the dielectric function of the material may have been dramatically altered by the leading edge of the pulse when those structures are imprinted, with consequences on the group-velocity dispersion (GVD). Moll and Gaeta [84] have shown that in anomalous GVD, collapse dynamics are modified and that multiple collapse can occur many diffraction lengths away from the initial collapse point, fitting with our observations. Nevertheless, further experimental work is needed to elucidate convincingly the mechanism leading to the formation of those features.

4.1.2 Energy dependence study in BK7

PCM and OTM observations in BK7

Phase contrast microscopy (PCM) and optical transmission microscopy (OTM) observations of laser-induced tracks in BK7 are presented in Fig. 4.1 for different laser energies ranging from 150 nJ to 11 μJ. In contrast with the observations made in a-SiO_2, the laser-generated imprints are almost undetectable in OTM. Nonetheless, the OTM observation is presented in Fig. 4.5. In the future, OTM observations will be presented only when bringing a substantial support to the discussion.

Discussion

The type of response is very different from what we reported for a-SiO_2. Firstly, in the experimental conditions of Fig. 4.5, no black stain could be observed. As expected from the results reported in [85, 86], the refractive index change Δn is mostly negative. The laser-induced tracks exhibit a teardrop-shaped, low density region surrounded by a dark shell.

N-BK7 is a multicomponent glass (see Sec. 3.4.3) in which chemistry indisputably plays an important role. In particular, BK7 contains alkaline ions (potassium oxide) which are determinant in that concerns the glass structure. Despite of their very small concentrations, ions with multiple valence that can be found in BK7 (titanium, calcium,...) also crucially influence the final glass structure. Under laser action, complex chemical and structural modifications take place. Our investigation tools (phase contrast microscopy and optical

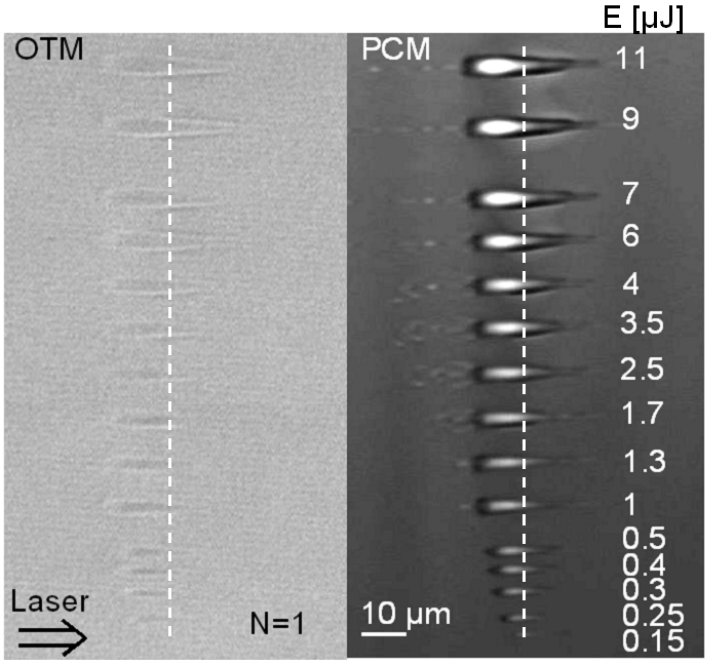

Figure 4.5: Phase contrast microscopy (PCM) and optical transmission microscopy (OTM) observations of laser-induced traces by a single pulse in BK7 for various laser beam energies. On the right column, laser pulse energies in μJ are specified. The dot line represents the estimated focal plane.

transmission microscopy) allow for a visualization of the final consequences of the irradiation on the refractive index of the target material, but do not allow for taking into account the respective role of the different chemical components.

Therefore, in absence of complementary analysis tools, we propose a scenario where thermal expansion and associated thermomechanical effects play a central role. This description is consistent with our observations and does not discard the importance of the chemistry-oriented description, as themomechanical properties are assuredly closely correlated with the mobility of ions.

When the laser energy has been coupled to the electronic system and transfered to the ions, the temperature of the material drastically increases. The low softening point of BK7 (560 °C) may imply that a phase transition possibly takes place. Upon thermal expansion, the heated material spontaneously flows away from the high energy density region and aggregates on the interface with the cold bulk, confined by the internal pressure of the cold material. This specificity in the material response is partly due to the huge difference (factor of about 15) between the respective coefficients of linear expansion in Bk7 and a-SiO_2.

A noteworthy feature is visible for energies higher than 1.3 μJ. The part of the trace close to laser exhibits a cloud of off-axis dots. Their formation corresponds to spots of high energy deposition, and can speculatively be the result of an interference pattern. For energies higher than 7 μJ, the location of the dots is restricted on axis, as observed in the case of fused silica.

4.1.3 Influence of spherical aberrations

A comprehensive theoretical study regarding the consequences of spherical aberrations on the beam focusing has already been developed in Sec. 3.2.2 but as we mentioned, the response of the material was not taken into account.

Experimental conditions and presentation of the OTM and PCM observations

Traces presented in Fig. 4.6 were generated with system II in BK7 and the laser induced imprints presented in Fig. 4.7 were generated with system I in amorphous fused silica. For both materials, the effect of spherical aberrations was enhanced by focusing the laser pulses at a distance of 500 μm of the air-glass interface.

Discussion

As expected from our previous theoretical work, the more noticeable effect is the dramatic elongation experienced by the focal volume. Hence, the energy deposition takes place over an extended region on the optical axis. As a major consequence, the local intensity dramatically

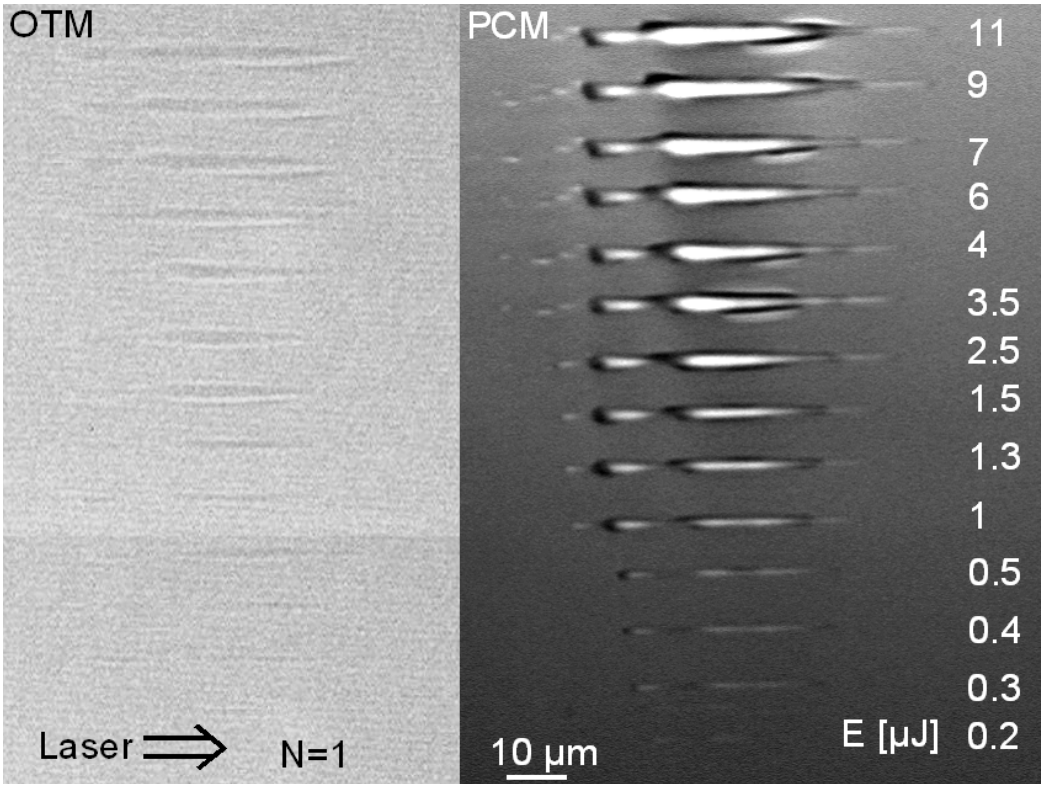

Figure 4.6: Aspect of fs laser-induced traces in BK7 in optical transmission microscopy (OTM) and in phase contrast microscopy (PCM). Aberrations are enhanced by focusing 0.5 mm into the bulk. On the right column, laser pulse energies in μJ are specified.

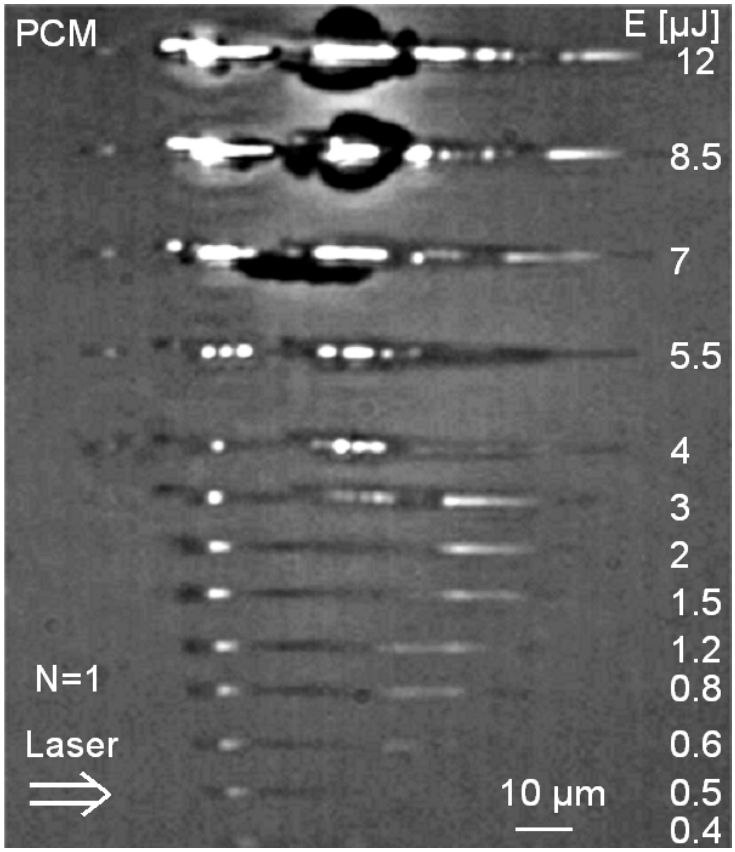

Figure 4.7: Aspect of fs laser-induced traces in a-SiO_2 in phase contrast microscopy (PCM). The optical transmission microscopy observation was not recorded. Aberrations are enhanced by focusing 0.5 mm into the bulk. On the right column, laser pulse energies in μJ are specified.

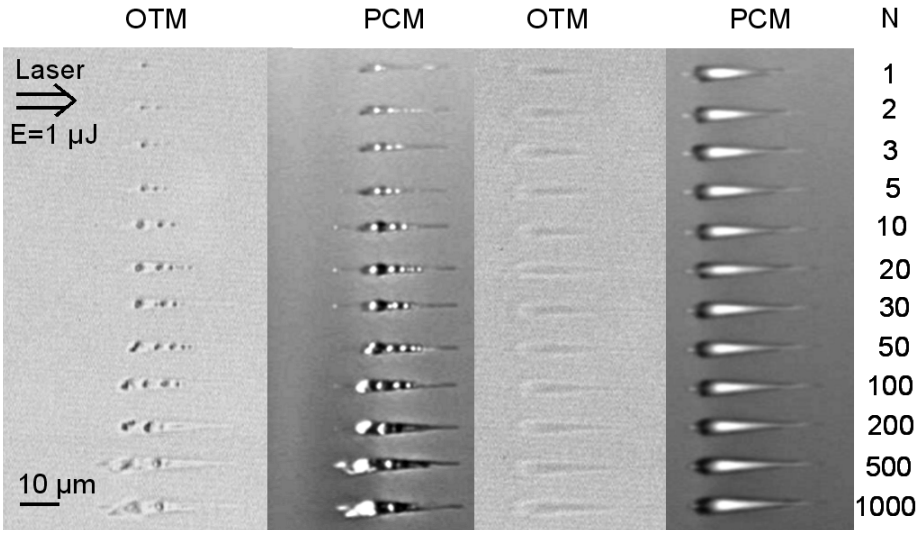

Figure 4.8: Aspect of fs laser-induced traces in a-SiO_2 (left) and Bk7 (right) for different numbers of shots per site in OTM and PCM. The maximal repetition rate is of 166 Hz. The laser pulse energy is 1 μJ. The number of shots per site (N) is indicated.

drops down and the laser pulse energy needed for initiating detectable bulk modifications logically increases. Liu and coworkers [65] proposed to use focus elongation upon aberrations to write waveguiding structures with controllable aspect ratio.

Practically, focus elongation is a challenging limitation to overcome for longitudinal waveguide writing but also for writing 2-dimensional arrays of waveguides. A promising way to beat wavefront destruction upon propagation is to use spatial adaptive beam profile control [87, 88].

4.2 Multipulse irradiation

4.2.1 Irradiation at low repetition rates in a-SiO_2 and BK7

Experimental conditions and presentation of the PCM and OTM observations

BK7 and a-SiO_2 samples are irradiated with system II, at a fixed laser pulse energy (E_{in} = 1μJ). The number of shots per site (N) is gradually increased. The time between two successive pulses is at least of 6 ms. In this way, each pulse interacts with a cold bulk. PCM and OTM images are presented in Fig. 4.8.

The difference between the response of BK7 and a-SiO_2 is striking. In BK7, the number of pulse does not seem to play a big role in the final morphology of the final track. The length and the global shape is not very different from N=1 to N=1000. Conversely, the

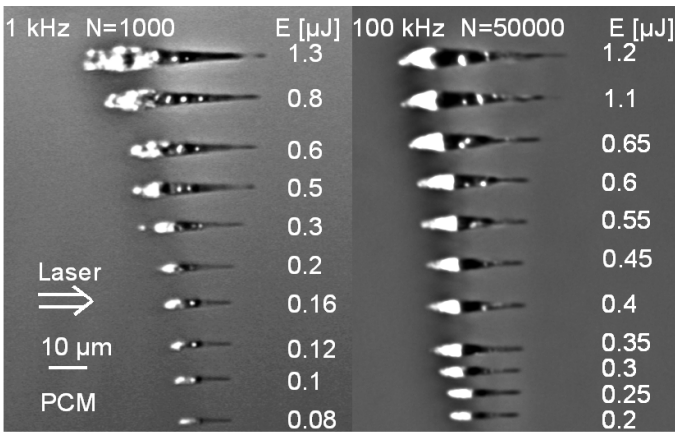

Figure 4.9: Aspect of fs laser-induced traces in a-SiO_2 for different repetition rates. Laser pulse energies in μJ are specified. The number of shots (N) is also indicated.

same study in fused silica shows a dramatic morphological evolution depending on N, with a saturation starting at N=500. When the number of pulses per site is increased, white bubble-like inclusions appear along the trace in PCM. Those inclusions are visible in OTM as well. Watanabe and coworkers [89] identified those bubbles as voids, and proposed a scenario in which voids move upon additional irradiation.

Figure 4.8 indisputably shows that incubation phenomena take place in amorphous silica where each shot modifies the material by inducing defects or, generally saying, previous long-living material modifications that alter gradually the absorption properties. As a consequence, the affected volume grows progressively from shot to shot.

4.2.2 Irradiation at high repetition rates (1kHz and 100 kHz) in a-SiO_2 and BK7

Experimental conditions and presentation of the PCM observations

The samples are now irradiated during 1s at a 1kHz repetition rate with system II and also during 0.5 s with system IV at a repetition rate of 100 kHz, for the comparison. PCM observations are presented in Fig. 4.9. The OTM images were not recorded.

The same irradiation sequences are applied to BK7. The structures visible in PCM are hardly detectable in OTM. Therefore, PCM images only are presented in Fig. 4.10.

Discussion

Figure 4.9 shows that the energy relaxation in amorphous fused silica is very similar at low and high repetition rates. Both types of traces show a morphology very similar to the

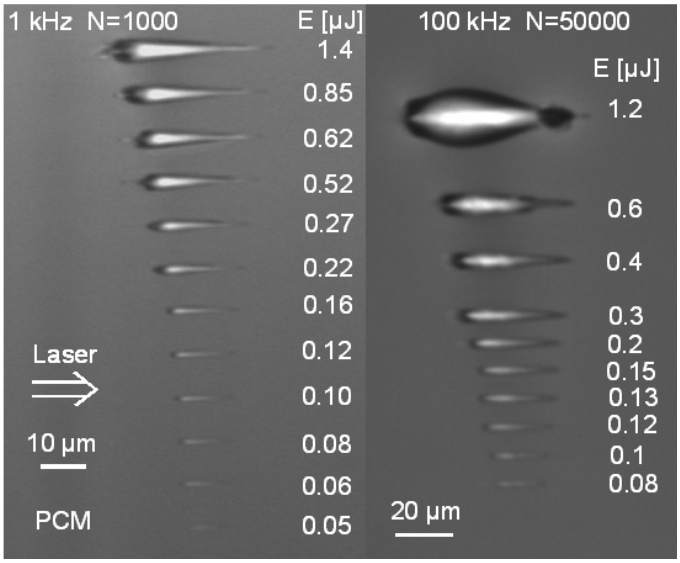

Figure 4.10: Aspect of fs laser-induced traces in BK7 for different repetition rates. Laser pulse energies in μJ are specified. The number of shots is also indicated. Note the difference of scale bars.

imprint for N=1000 shots at a 100 Hz repetition rate presented in Fig. 4.8.

In BK7 (Fig. 4.10), two different types of response emerge. For laser pulse energies lower than 1 μJ, the teardrop morphology observed previously is conserved, although a comparison with Fig. 4.5 reveals that the global size increases under high repetition rate irradiation. For laser pulse energies above 1 μJ, a new type of interaction takes place. The trace is more elongated on the transverse direction and the black shell surrounding the white region is much thicker than previously, suggesting an increasing hydrodynamic activity. We assumed initially that such a different behavior could also originate from the big difference in terms of number of pulse per site. To clarify this point, N = 50000 shots were fired on the same site, but with a 1 kHz repetition rate (Fig. 4.11). Those results indisputably show that the material does not have enough time to relax and attain a frozen state before the arrival of the next pulse when the distance between two consecutive pulses is of 10 μs only. Therefore, each pulse couples in a softened material and results in considerable inelastic flow toward the extremities.

4.2.3 Conclusion and perspectives

As a conclusion, BK7 and SiO_2 exhibit very different behaviors. Whereas pure amorphous silica shows a high sensitivity to the number of pulses but only minor variations when irradiated at high or low repetition rates, BK7 exhibits systematically a thermal-like response

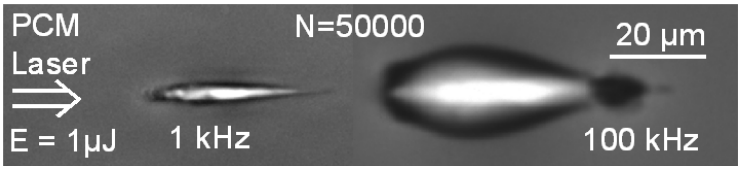

Figure 4.11: Aspect of fs laser-induced traces in BK7 for different repetition rates. The number of shots is N=50000. The laser pulse energy is 1.2 μJ. The repetition rates are indicated.

dominated by heat expansion. When high repetition rates (>100 kHz) are used, accumulation effects from pulse to pulse takes place even at moderated laser pulse energies.

4.3 Irradiation with chirped pulses

4.3.1 Threshold dependence versus chirp

Given the influence of the nonlinear effects in the final energy deposition pattern, the pulse duration is expected to be a very important input parameter. Additionally, the sequence of frequencies under the temporal envelope may influence the balance of different mechanisms. A previous study about the damage thresholds on the surface of dielectrics [90] reports a 20 % lowering of the damage thresholds for negatively chirped pulses, with the following interpretation. Downchirped pulses (i.e. high energy photons come first) produce more free carriers by multiphoton ionization (MPI) during the leading edge of the pulse. An increase in the number of seed electrons being very beneficial for the subsequent collisional processes, the global amount of free carriers created generated throughout the pulse is substantially higher for down-chirped pulses. In this section, we propose to verify whether one can observe the same phenomenon in the bulk of amorphous silica, employing a dark-field scattering technique.

Experiment

A He-Ne Laser propagates collinearly with the beam delivered by system II. The sample is placed under the microscope, the light source of the microscope is off. A single pulse is carefully selected and focused in the bulk of the sample. The laser pulse energy can be continuously tuned with the help of a half wave plate associated with a polarizer. After the bulk irradiation, the He-Ne is turned on and a picture is recorded. The threshold is defined as the lowest energy for recording a signal. This technique appears to be very sensitive for measuring thresholds of structural modifications invisible in PCM and in OTM as well.

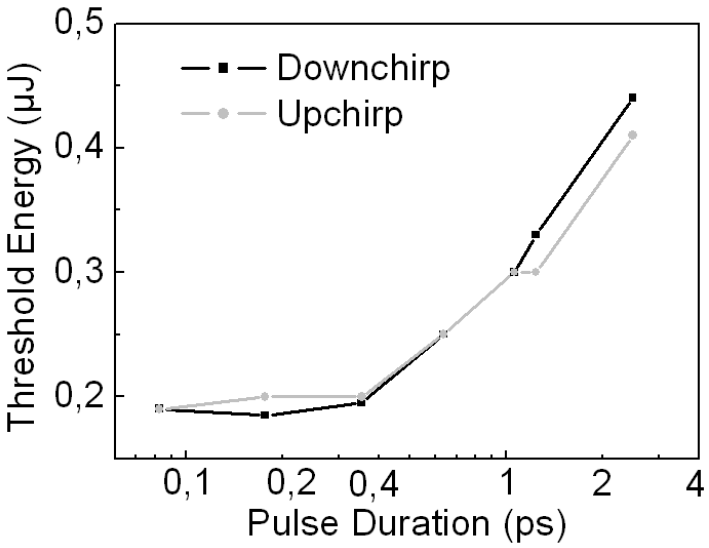

Figure 4.12: Energy threshold for bulk modification versus pulse duration. Down- and up-chirped pulses have been focused in the bulk of fused silica.

Results and discussion

Our experimental investigations (Fig. 4.12) do not show any significant influence of the chirp sign on the damage threshold. Plausibly, it may be because in the bulk, nonlinear propagation is important and not straight forward predictable. In Sec. 2.2.3, we saw that new frequencies could be generated by self-phase modulation. Additionally, the axial intensity can be changed differently for different chirp directions upon nonlinear propagation. Obviously, the effects of nonlinear propagation do not play any role when studying the damage on the surface, in the experimental conditions of Louzon et al. [90]. This may explain why we can not observe any threshold lowering depending on the chirp direction.

4.3.2 Energy deposition in the picosecond regime

Experiment

We now investigate the morphology of traces induced by picosecond laser pulses. The study was carried out in the same way as before, i.e. by controlling the amount of chirp, the pulse duration was gradually increased to pulse durations up to the picosecond range.

Results and discussion

Results are shown in Fig. 4.13 for down-chirped pulses in BK7 and a-$Si0_2$. The PCM images are very similar in the case of a positive chirp. Strikingly, the main differences we emphasized

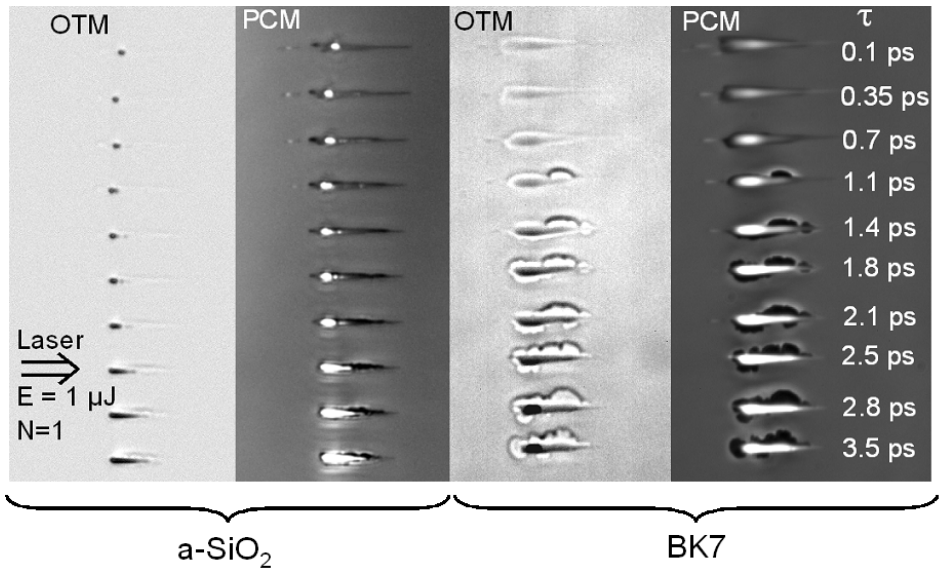

Figure 4.13: Aspect of traces induced by down-chirped pulses in fused silica (left) and BK7 (right) in optical transmission microscopy (OTM) and phase contrast microscopy (PCM). The laser pulse energy is 1 μJ. The laser pulse durations (τ) are given in ps.

between modifications induced in BK7 and a-SiO_2 vanish when the pulse duration enters the picosecond range. Irrespective of the nature of the material, the global aspect of the laser-induced tracks exhibits an interesting resemblance with the thermal response we described in Sec. 4.1.2 for BK7 under standard ultrafast irradiation conditions. A noticeable difference is the onset of a shock-affected region even for a moderated laser pulse energy. Some simulations have been carried out using the model presented in Sec. 2.4.1. The excitation footprints at the end of the irradiation sequence are presented in Fig. 4.14. A comparison with Fig. 4.3 reveals several distinctive elements. Although the overall absorbed energy is lower than in the femtosecond case (about 30% against 50% with an ultrashort pulse), the energy deposition is more confined along the optical axis. The major reason is that the trailing edge of the pulse does not experience as much plasma defocusing as in the previous case. As a consequence, Fig. 4.14 (b) shows that the energy is deposited in a very homogeneous way. Consequently, a uniform population of free electrons is generated (see Fig. 4.14 (d)) and further heated, leading to a global material expansion in the affected volume. As expected, the incident intensity distribution is affected by the pulse elongation and the high intensity channel observed before disappears.

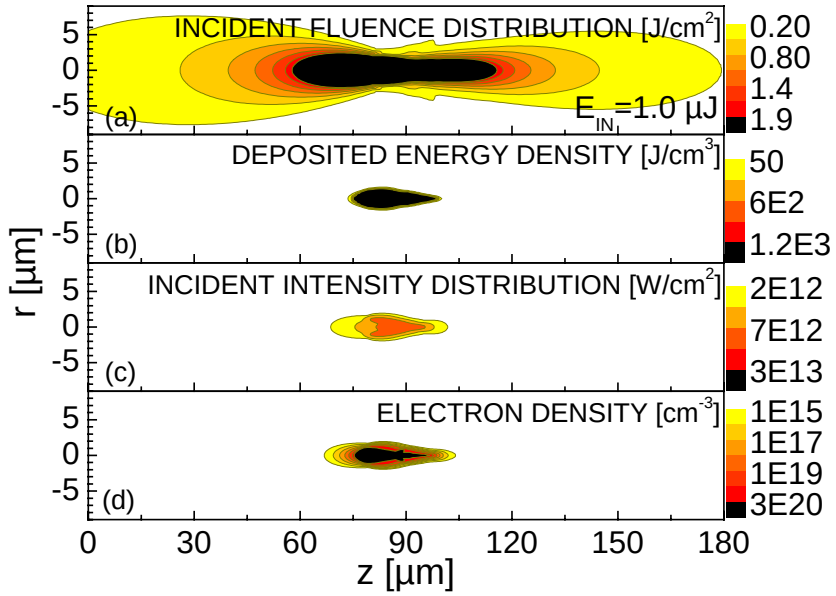

Figure 4.14: Excitation footprints in a-SiO_2 at the end of a 2 ps irradiation pulse. (a) incident fluence (J/cm^2); (b) absorbed energy (J/cm^3); (c) peak intensity distribution (W/cm^2); (d) peak electronic density (cm^{-3}).

4.4 Conclusion

The following points have been demonstrated in this chapter, and are worth being highlighted.

At first, we note a drastic difference in the response of BK7 and a-SiO_2 under laser irradiation, emphasized by the use of phase contrast microscopy. While the response of BK7 seems to be dominated by thermal expansion resulting in the onset of a low density material, the response of a-SiO_2 looks more enigmatic. After exposure at moderate laser energies, mainly two regions are detectable. A low density region, identified as a void, and a filament of higher refractive index than the pristine bulk. Solving the nonlinear Schrödinger equation allowed us to assign the formation of this void to a high energy exposure. Although a speculative scenario was proposed to explain the origin of the filament, the formation of this feature has to be further studied.

Another noticeable difference between BK7 and a-SiO_2 is their response to a multipulse irradiation sequence. Incubation effects clearly appear in a-SiO2 up to approximately one thousand shots per site, but we could not detect any noticeable sensitivity to the repetition rate, at least up to 100 kHz. Conversely, the response of BK7 is practically not affected by the number of shots per site. We demonstrated that instead, the repetition rate is the critical parameter, suggesting that thermal effects play a dominant role.

Finally, the studies involving different amounts and directions of chirp clearly show that the modification threshold in the bulk does not depend on the chirp direction, but rather on the pulse duration. When picosecond duration pulses are used, defocussing on the electron-hole plasma is limited and the laser energy is deposited in a confined region, in the vicinity of the optical axis.